Article

Electromechanics of a Redox-Active Rotaxane in a Monolayer Assembly on an Electrode

Eugenii Katz, Oleg Lioubashevsky, and Itamar Willner

J. Am. Chem. Soc., **2004**, 126 (47), 15520-15532• DOI: 10.1021/ja045465u • Publication Date (Web): 09 November 2004

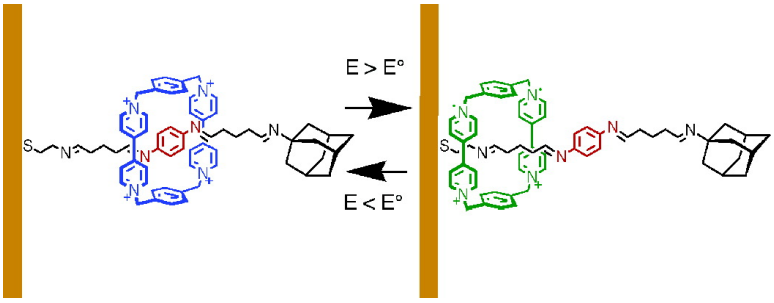

More About This Article

Additional resources and features associated with this article are available within the HTML version:

- Supporting Information
- Links to the 15 articles that cite this article, as of the time of this article download
- Access to high resolution figures
- Links to articles and content related to this article
- Copyright permission to reproduce figures and/or text from this article

View the Full Text HTML

J|A|C|S
ARTICLES
Published on Web 11/09/2004

Electromechanics of a Redox-Active Rotaxane in a Monolayer Assembly on an Electrode

Eugenii Katz, Oleg Lioubashevsky, and Itamar Willner*

Contribution from the Institute of Chemistry, The Hebrew University of Jerusalem, Jerusalem 91904, Israel

Received July 28, 2004; E-mail: willnea@vms.huji.ac.il

Abstract: A rotaxane monolayer consisting of the cyclophane, cyclobis(paraquat-*p*-phenylene) (**2**), threaded on a "molecular string" that includes a π-donor diiminobenzene unit and stoppered by an adamantane unit is assembled on a Au electrode. The surface coverage of the electroactive cyclophane unit, $E^{\circ} = -0.43$ V vs SCE, corresponds to 0.8×10^{-10} mol·cm^{-2}. The cyclophane (**2**) is structurally localized on the molecular string by generating a π-donor−acceptor complex with the diiminobenzene units of the molecular string. The cyclophane (**2**) acts as a molecular shuttle, revealing electrochemically driven mechanical translocations along the molecular wire. Reduction of the cyclophane (**2**) to the respective biradical−dication results in its dissociation from the π-donor site, and the reduced cyclophane is translocated toward the electrode. Oxidation of the reduced cyclophane reorganizes **2** on the π-donor-diiminobenzene sites. The positions of the oxidized and reduced cyclophane units are characterized by chronoamperometric and impedance measurements. Using double-step chronoamperometric measurements the dynamics of the translocation of the cyclophane units on the molecular string is characterized. The reduced cyclophane moves toward the electrode with a rate constant corresponding to $k_1 = 320$ s^{-1}, whereas the translocation of the oxidized cyclophane from the electrode to the π-donor binding site proceeds with a rate constant of $k_2 = 80$ s^{-1}. Also, in situ electrochemical/contact angle measurements reveal that the electrochemically driven translocation of the cyclophane on the molecular string provides a means to reversibly control the hydrophilic and hydrophobic properties of the surface. The latter system demonstrates the translation of a molecular motion into the macroscopic motion of a water droplet.

Introduction

Miniaturization of devices to the molecular level or nanoscale dimensions is one of the most challenging research subjects in modern science.[1] Molecular and supramolecular assemblies could operate as parts of molecular machinery units capable of performing diverse mechanical functions.[2] Basic molecular mechanical components such as levers, rotors,[3] and translational transporters[4] are well known, and molecular-based machinery systems of higher degree of complexity have been also reported.[5] Progress in tailoring molecular machines may have important implications in molecular-based logic gates,[6] computer technologies,[7] sensory methods,[8] and nanoscale bioengineering.[9] Tailoring of molecular machines requires integration of chemical components with a solid transducer to the extent that the molecular assembly communicates with its macroscopic environment. That is, the molecular machine is activated or blocked by external signals, such as electrical or photonic stimuli, and

(1) (a) *Molecular Electronic Devices*; Carter, F. L., Siatkowsky, R. E., Woltjien, H., Eds.; Elsevier: Amsterdam, 1988. (b) *Nanosystems, Molecular Machinery, Manufacturing and Computation*; Drexler, K. E., Ed.; Wiley: New York, 1992.

(2) (a) Balzani, V.; Gómex-López, M.; Stoddart, J. F. *Acc. Chem. Res.* **1998**, *31*, 405−414. (b) Shipway, A. M.; Katz, E.; Willner, I. In *Structure and Bonding*; Sauvage J.-P., Ed.; Springer-Verlag: Berlin, 2001; Vol. 99, pp 237−281. (c) Balzani, V.; Credi, A.; Raymo, F. M.; Stoddart, J. F. *Angew. Chem., Int. Ed.* **2000**, *39*, 3348−3391. (d) Balzani, V.; Credi, A.; Venturi, M. *Molecular Devices and Machines−A Journey into the Nano World*; Wiley-VCH: Weinheim, 2003. (e) Brouwer, A. M.; Frochot, C.; Gatti, F. G.; Leigh, D. A.; Mottier, L.; Paolucei, F.; Roffia, S.; Wurpel, G. W. H. *Science* **2001**, *291*, 2124−2128. (f) Stanier, C. A.; Alderman, S. J.; Claridge, T. D. W.; Anderson, H. L. *Angew. Chem., Int. Ed.* **2002**, *41*, 1769−1772. (g) Pomeranc, D.; Jouvenot, D.; Chambron, J.-C.; Collin, J.-P.; Heitz, V.; Sauvage, J.-P. *Chem. Eur. J.* **2003**, *9*, 4247−4254. (h) Leigh, D. A.; Wong, J. K. Y.; Dehez, F.; Zerbetto, F. *Nature* **2003**, *424*, 174−179. (i)) Bottari, G.; Dehez, F.; Leigh, D. A.; Nash, P. J.; Perez, E. M.; Wong, J. K. Y.; Zerbetto, F. *Angew. Chem., Int. Ed.* **2003**, *42*, 5886−5889. (j) Hernandez, R.; Tseng, H.-R.; Wong, J. W.; Stoddart, J. F.; Zink, J. I. *J. Am. Chem. Soc.* **2004**, *126*, 3370−3371. (k) Shipway, A. N.; Willner, I. *Acc. Chem. Res.* **2001**, *34*, 421−432.

(3) (a) Guenzi, A.; Johnson, C. A.; Cozzi, F.; Mizlow, K. *J. Am. Chem. Soc.* **1983**, *105*, 1438−1448. (b) Kelly, T. R.; Bowyer, M. C.; Bhaskar, K. V.; Bebbington, D.; Garcia, A.; Lang, F.; Kim, M. H.; Jette, M. P. *J. Am. Chem. Soc.* **1994**, *116*, 3657−3658. (c) Schoevaars, A. M.; Kruizinga, W.; Zijlstra, R. W. J.; Veldman, N.; Spek, A. L.; Feringa, B. L. *J. Org. Chem.* **1997**, *15*, 44943−44948. (d) Koumura, N.; Zijlstra, R. W. J.; van Delden, R. A.; Harada, N.; Feringa, B. L. *Nature* **1999**, *401*, 152−155. (e) Kelly, T. R.; Tellitu, I.; Sestelo, J. P. *Angew. Chem., Int. Ed. Engl.* **1997**, *36*, 1866−1868.

(4) Philp, D.; Stoddart, J. F. *Angew. Chem., Int. Ed. Engl.* **1996**, *35*, 1155−1196.

(5) (a) Menzer, S.; White, A. J. P.; Williams, D. J.; Belohradsky, M.; Hamers, C.; Raymo, F. M.; Shipway, A. N.; Stoddart, J. F. *Macromolecules* **1998**, *31*, 295−307. (b) Ashton, P. R.; Baldoni, V.; Balzani, V.; Claessens, C. G.; Credi, A.; Hoffman, H. A. D.; Raymo, F. M.; Stoddart, J. F.; Venturi, M.; White, A. J. P.; Williams, D. J. *Eur. J. Org. Chem.* **2000**, *7*, 1121−1130. (c) Amabilino, D. B.; Asakawa, M.; Ashton, P. R.; Ballardini, R.; Balzani, V.; Belohradsky, M.; Credi, A.; Higuchi, M.; Raymo, F. M.; Shimizu, T.; Stoddart, J. F.; Venturi, M.; Yase, K. *New J. Chem.* **1998**, *22*, 959−972.

(6) De Silva, A. P.; Gunarante, H. Q. N.; McCoy, C. P. *Nature* **1993**, *364*, 42−44.

(7) *Nanosystems, Molecular Machinery, Manufacturing and Computation*; Drexler, K. E., Ed.; Wiley: New York, 1992.

(8) Schierbaum, K. D.; Weiss, T.; Thoden van Velzen, E. U.; Engkersen, J. F. J.; Reinhoudt, D. A.; Göpel, W. *Science* **1994**, *265*, 1413−1415.

(9) Willner, I. *Acc. Chem. Res.* **1997**, *30*, 347−356.

10.1021/ja045465u CCC: $27.50

the state of the machine reflected by the structural position and chemical state is electronically transduced to the surroundings. Molecular switches[10] and molecular shuttles[11] were assembled in solution in an attempt to mimic functions of macroscopic machinery. In these systems external, photonic,[12] electrical,[13] or pH signals[14] were used to stimulate switchable binding of ions[15] or neutral substrates,[16] switchable formation of donor−acceptor complexes,[13] switchable electrochemical and bioelectrochemical properties,[12] and signal-triggered translocation of molecular components.[17] The signal-triggered functions of these molecular assemblies were spectroscopically characterized in the bulk solution. Extensive recent efforts were directed to integrate these photoswitchable chemical assemblies with transducers in order to tailor molecular devices. Specifically, electrical transduction of photonic information recorded by photosensitive monolayers on electrode supports was used to develop molecular optoelectronic systems.[18] Photochemical activation of redox functions of monolayers,[18b] application of photoisomerizable monolayers assembled on electrode surfaces as 'command interfaces' for controlling interfacial electron transfer,[19] and the functionalization of electrodes with receptor sites exhibiting controlled affinity to photoisomerizable redox-active substrates[20] were used as a general means to organize molecular optoelectronic devices.

Rotaxanes are interesting supramolecular structures,[21] and redox-active rotaxanes assembled on surfaces were used as molecular electronic[22] and optoelectronic[23] devices. Recently, we reported on a redox-active rotaxane assembled on a Au electrode that operated as a shuttling electron relay transporting electrons from glucose oxidase to the electrode support.[24] Transient electrochemical methods were applied to analyze the kinetics of the redox-active rotaxane translocation along the molecular string.[22c,24] Here we report on the synthesis of a surface-confined redox-active rotaxane system that reveals switchable and controlled interfacial properties, such as switchable electron-transfer kinetics at the electrode, controlled interfacial capacitance, and modulated wettability. Chronoamperometry and impedance spectroscopy are used as electrochemical methods to probe the changes of the interfacial properties of the electrode upon the electrochemically induced rotaxane translocation on a molecular string associated with the electrode in a monolayer configuration.

Experimental Section.

Chemicals. Cyclobis(paraquat-*p*-phenylene) (termed as the "cyclophane") was synthesized and purified as described before.[25] All other chemicals, including pyrroloquinoline quinone (PQQ), 4-(2-hydroxyethyl)-piperazine-1-ethanesulfonic acid sodium salt (HEPES), 1-ethyl-3-(3-dimethylaminopropyl)-carbodiimide (EDC), glutaric dialdehyde, potassium ferrocyanide, potassium ferricyanide, and 1-amino-adamantane, were purchased from Aldrich and used as supplied. Ultrapure water from Seralpur Pro 90 CN source was used in all experiments.

Modification of Electrodes. A Au-coated (50 nm gold layer) glass plate (Analytical-μSystem, Germany) was used as a working electrode (1.13 cm^2 area, roughness factor ca. 1.2, exposed to the solution). The Au electrodes were cleaned in boiling ethanol for 2 min. Cystamine was self-assembled on the electrode to yield the amino-functionalized surface as described before.[26] The resulting amino-functionalized electrodes were reacted with glutaric dialdehyde, 10% v/v, for 20 min. This and all other modification steps were performed in 0.1 M phosphate buffer, pH = 7.0. After each modification step the electrodes were rinsed with water. The aldehyde-functionalized electrodes were reacted with *p*-phenylenediamine (**1**), 10 mM, for 20 min. The *p*-phenylenediamine-functionalized electrodes were again reacted with glutaric dialdehyde, 10% v/v, for 20 min, yielding diiminobenzene units that are incorporated into the molecular string. To analyze the surface amino groups appearing and disappearing upon the modification steps, sample electrodes after each modification step were reacted with PQQ, 1 mM, in 0.1 M HEPES buffer, pH = 7.2, in the presence of EDC, 1 mM, for 2 h. The PQQ units covalently attached to the amino groups were assayed by cyclic voltammetry.[26] The electrodes functionalized with the diiminobenzene groups were reacted with the cyclophane (**2**), 0.3 mM, to generate the equilibrium donor−acceptor complex of the rotaxane structure. The electrode containing the surface donor−acceptor complex was further reacted with 1-amino-adamantane (**3**), 0.5 mM, for 20 min in order to generate a stopper on the molecular string. The reaction with 1-amino-adamantane was performed in the presence of **2**, 0.3 mM, to maintain the reversible donor−acceptor complex on the surface. All modification steps were repeated on a Au−quartz QCM electrode (9 MHz) in order to follow microgravimetrically the surface coverage of the components bound to the surface.

Electrochemical, Microgravimetric, and Contact Angle Measurements. A conventional three-electrode cell, consisting of the modified Au working electrode, a glassy carbon auxiliary electrode, and a saturated calomel reference electrode (SCE) connected to the working

(10) Zelikovich, L.; Libman, J.; Shanzer, A. *Nature* **1995**, *374*, 790−792.
(11) (a) Bissell, R. A.; Cordova, E.; Kaifer, A. E.; Stoddart, J. F. *Nature* **1994**, *369*, 133−137. (b) Lane, A. S.; Leigh, D. A.; Murphy, A. *J. Am. Chem. Soc.* **1997**, *119*, 11092−11093. (c) Long, B.; Nikitin, K.; Fitzmaurice, *J. Am. Chem. Soc.* **2003**, *125*, 15490−15498.
(12) (a) Kawai, S. H.; Gilat, S. L.; Ponsinet, R.; Lehn, J.-M. *Chem. Eur. J.* **1995**, *1*, 285−293. (b) Blonder, R.; Katz, E.; Willner, I.; Wray, V.; Bückmann, A. F. *J. Am. Chem. Soc.* **1997**, *119*, 11747−11757.
(13) Willner, I.; Marx, S.; Eichen, Y. *Angew. Chem., Int. Ed. Engl.* **1992**, *31*, 1243−1244.
(14) Katz, E.; Lion-Dagan, M.; Willner, I. *J. Electroanal. Chem.* **1996**, *408*, 107−112.
(15) Winkler, J. D.; Deshayes, K.; Shao, B. In *Bioorganic Photochemistry—Biological Application of Photochemical Switches*; Morrison, H., Ed.; Wiley: New York, 1993; Vol. 2, p 169.
(16) Würthner, F.; Rebek, J. *Angew. Chem., Int. Ed. Engl.* **1995**, *34*, 446−448.
(17) Shinkai, S.; Minami, T.; Kusano, T.; Manabe, O. *J. Am. Chem. Soc.* **1982**, *104*, 1967−1972.
(18) (a) Liu, Z. F.; Hashimoto, K.; Fujishima, A. *Nature* **1990**, *347*, 658−660. (b) Doron, A.; Portnoy, M.; Lion-Dagan, M.; Katz, E.; Willner, I. *J. Am. Chem. Soc.* **1996**, *118*, 8937−8944.
(19) Doron, A.; Katz, E.; Tao, G. L.; Willner, I. *Langmuir* **1997**, *13*, 1783−1790.
(20) Ranjit, K. T.; Marx-Tibbon, S.; Ben-Dov, I.; Willner, I. *Angew. Chem., Int. Ed. Engl.* **1997**, *36*, 147−150.
(21) (a) Fyfe, M. C. T.; Stoddart, J. F. *Acc. Chem. Res.* **1997**, *30*, 393−401. (b) Tseng, H. R.; Vignon, S. A.; Stoddart, J. F. *Angew. Chem., Int. Ed.* **2003**, *42*, 1491−1495. (c) Rowan, S. J.; Stoddart, J. F. *Polym. Adv. Technol.* **2002**, *13*, 777−787. (d) Rowan, S. J.; Cantrill, S. J.; Cousins, G. R. L.; Sanders, J. K. M.; Stoddart, J. F. *Angew. Chem., Int. Ed.* **2002**, *41*, 898−952.
(22) (a) Lahav, M.; Shipway, A. N.; Willner, I. *J. Chem. Soc., Perkin Trans. 2* **1999**, *9*, 1925−1931. (b) Kharitonov, A. B.; Shipway, A. N.; Willner, I. *Anal. Chem.* **1999**, *71*, 5441−5443. (c) Willner, I.; Pardo-Yissar, V.; Katz, E.; Ranjit, K. T. *J. Electroanal. Chem.* **2001**, *497*, 172−177. (d) Collier, C. P.; Wong, E. W.; Belohradsky, M.; Raymo, F. M.; Stoddart, J. F.; Kuekes, P. J.; Williams, R. S.; Heath, J. R. *Science* **1999**, *285*, 391−394. (e) Luo, Y.; Collier, C. P.; Jeppesen, J. O.; Nielsen, K. A.; Delonno, E.; Ho, G.; Perkins, J.; Tseng, H. R.; Yamamoto, T.; Stoddart, J. F.; Heath, J. R. *ChemPhysChem* **2002**, *3*, 519−525. (f) Tseng, H.-R.; Wu, D.; Fang, N. X.; Zhang, X.; Stoddart, J. F. *ChemPhysChem* **2004**, *5*, 111−116. (g) Weber, N.; Hamann, C.; Kern, J.-M.; Sauvage, J.-P. *Inorg. Chem.* **2003**, *42*, 6780−6792.
(23) (a) Sheeney-Haj-Ichia, L.; Willner, I. *J. Phys. Chem. B* **2002**, *106*, 13094−13097. (b) Asakawa, M.; Ashton, P. R.; Balzani, V.; Brown, C. L.; Credi, A.; Matthews, O. A.; Newton, S. P.; Raymo, F. M.; Shipway, A. N.; Spencer, N.; Quick, A.; Stoddart, J. F.; White, A. J. P.; Williams, D. J. *Chem. Eur. J.* **1999**, *5*, 860−875. (c) Ashton, P. R.; Balzani, V.; Kocian, O.; Prodi, L.; Spencer, N.; Stoddart, J. F. *J. Am. Chem. Soc.* **1998**, *120*, 11190−11191.
(24) Katz, E.; Sheeney-Ichia, L.; Willner, L. *Angew. Chem., Int. Ed.* **2004**, *43*, 3292−3300.
(25) Asakawa, M.; Dehaen, W.; Labbe, G.; Menzer, S.; Nouwen, J.; Raymo, F. M.; Stoddart, J. F.; Williams, D. J. *Org. Chem.* **1996**, *61*, 9591−9595.
(26) (a) Katz, E.; Schlereth, D. D.; Schmidt, H.-L. *J. Electroanal. Chem.* **1994**, *367*, 59−70. (b) Katz, E.; Schlereth, D. D.; Schmidt, H.-L.; Olsthoorn, A. J. J. *J. Electroanal. Chem.* **1994**, *368*, 165−171.

volume with a Luggin capillary, was used for the electrochemical measurements. All potentials are reported with respect to the SCE. Argon bubbling was used to remove oxygen from the solution in the electrochemical cell. The cell was placed in a grounded Faraday cage. Cyclic voltammetry, chronoamperometry, and impedance spectroscopy were performed using an electrochemical analyzer (model 6310, EG&G) connected to a personal computer (EG&G 398 software for impedance spectroscopy or EG&G 270/250 software for cyclic voltammetry and chronoamperometry). The *RC* cell/instrument time constant was assumed as the fastest component in the current decay during chronoamperometric measurements, and this is estimated to be shorter than 400 ns. The interfacial kinetics was measured only at times greater than about 5−10 *RC*. Biexponential analysis of the current decays and smoothing of the semilogarithmic plots were performed using KaleidoGraph 3.0 software with a Macintosh LSIII computer. Fitting of the experimental decay curves was performed using the general relation $A_1 \exp(-k_1 t) + A_2 \exp(-k_2 t)$. For all fitting procedures the correlation factor was $R > 0.98$. The electrochemical measurements were carried out in 0.1 M phosphate buffer, pH 7.0, as a background electrolyte, unless stated otherwise, at ambient temperature (25 ± 2 °C). The electrochemical measurements at variable pH values were performed in 0.1 M Britton−Robinson buffer titrated with HCl or KOH directly in the electrochemical cell to obtain the required pH values in a broad region. The Faradaic impedance spectra of the redox-active monolayer-functionalized electrodes were recorded upon application of the bias potentials corresponding to −0.33 or −0.53 V, while applying a 5 mV alternative voltage in the frequency range from 1 Hz to 10 kHz at −0.33 V and 1 Hz to 100 kHz at −0.53 V. The Faradaic impedance spectra are plotted in the form of complex plane diagrams, C_{im} vs C_{re} (Cole−Cole plots). The Faradaic impedance measurements in the presence of the diffusional redox probe were carried out in the presence of a 10 mM $K_3[Fe(CN)_6]/K_4[Fe(CN)_6]$ 1:1 mixture and performed in 0.1 M Britton−Robinson buffer while biasing the electrode at 0.17 V and applying a 5 mV alternative voltage in the frequency range from 1 Hz to 10 kHz. The Faradaic impedance spectra measured in the presence of the diffusional redox probe are plotted in the form of complex plane diagrams, Z_{im} vs Z_{re} (Nyquist plots). The experimental impedance spectra were fitted using appropriate electronic equivalent circuits. For this purpose commercial software (Zview, version 2.1b, Scribner Associates, Inc.) was employed.

A QCM analyzer (Fluke 164T multifunction counter, 1.3 GHz, TCXO) and quartz crystals (AT-cut, 9 MHz, Seiko) sandwiched between two Au electrodes (area 0.196 cm^2, roughness factor ca. 3.2) were employed for the microgravimetric analyses in air. The QCM crystals were calibrated by electropolymerization of aniline in 0.1 M H_2SO_4 and 0.5 M Na_2SO_4 electrolyte solution, followed by coulometric assay of the resulting polyaniline film and relating the crystal frequency changes to the electrochemically derived polymer mass.[27]

Static in situ contact angle electrochemical measurements were performed using a droplet (10 ± 1 μL) of 0.1 M phosphate buffer solution, pH 7.0, on the modified Au electrode using a CAM2000 optical contact angle analyzer (KSV Instruments) and an EG&G, model 283, potentiostat. Thin silver and platinum wires (both with a diameter of 0.1 mm) were introduced into the droplet and used as a quasi-reference electrode and a counter electrode, respectively. Such thin wires were chosen to prevent distortion of the droplets. The Ag quasi-reference electrode was calibrated vs SCE by performing cyclic voltammetry of methyl viologen,[26a] which has a well-known redox potential, $E° = -0.687$ V vs SCE, and then the potentials were reported vs SCE. The contact angle measurements were performed by applying potential values corresponding to −0.33 or −0.53 V on the modified Au support. To extract the precise contact angle values, the droplet images were fitted using a software based on the Young−Laplace equation (KSV Instruments).[28] The contact angle values were determined with a precision of ±0.5°. The droplet was under an inert atmosphere generated by a flow of Ar gas through a funnel placed at a distance of 3 cm above the droplet. The experiments were performed within short time intervals (less than 2 min) in order to prevent droplet evaporation.

Scheme 1. Assembly of Interlocked Cyclophane (**2**) on a Molecular String Associated with an Electrode[a]

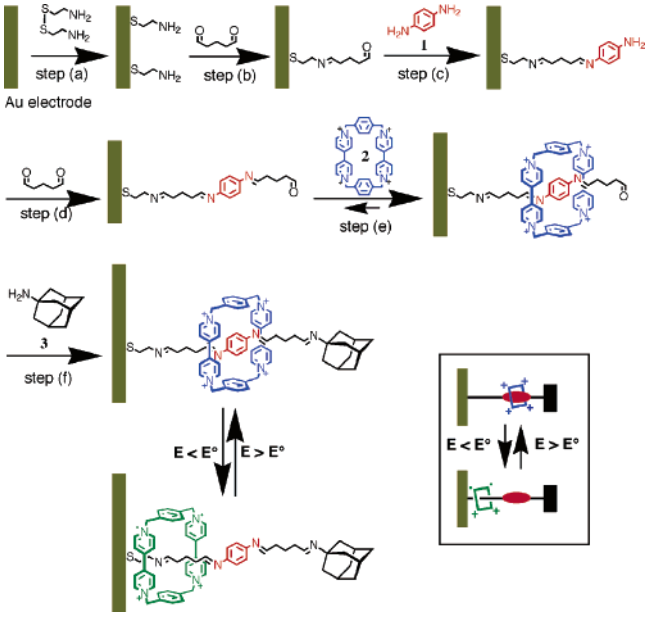

[a] Inset: Electrochemically induced translocation of the cyclophane upon reduction or oxidation.

Results and Discussions

Scheme 1 depicts the stepwise assembly of the rotaxane system on the gold electrode. Cystamine was self-assembled as a monolayer on the Au electrode, step a. The resulting amino-functionalized electrode was then reacted with glutaric dialdehyde, step b, and the obtained monolayer was reacted with 1,4-diaminobenzene (**1**), step c, to yield the iminophenylamino-functionalized monolayer. The generated monolayer was further reacted with glutaric dialdehyde, step d, and then interacted with the electron-acceptor cyclobis(paraquat-*p*-phenylene) (**2**) step e, to yield the supramolecular donor−acceptor complex with the diiminobenzene electron-donating units. The resulting supramolecular structure was then stoppered with 1-amino-adamantane (**3**), step f, to generate the rotaxane structure that includes the cyclophane (**2**) threaded on the stoppered wire. The stepwise modification of the Au electrode surface was confirmed by the covalent binding of PQQ to the amino-group-terminated monolayers generated after modification steps a and c.[24] The surface coverage of the amino groups on the Au surface was estimated to be 1×10^{-10} mol·cm^{-2} since the PQQ surface coverage derived from the cyclic voltammograms is the same for the two structures of the amino-terminated monolayers. On the other hand, the monolayers that lack the amino groups (after steps b and d) did not react with PQQ, indicating quantitative yields in the respective reactions on the surface. The amounts of the surface-bound molecular components upon each step of the electrode modification, ca. 1×10^{-10} mol·cm^{-2}, were also

(27) Baba, A.; Tian, S.; Stefani, F.; Xia, C.; Wang, Z.; Advincula, R. C.; Johannsmann, D.; Knoll, W. *J. Electroanal. Chem.* **2004**, *562*, 95−103.

(28) (a) Jennings, J. W.; Pallas, N. R. *Langmuir* **1988**, *4*, 959−967. (b) Van Oss, C. J.; Good, R. J.; Chaudhury, M. K. *Langmuir* **1988**, *4*, 884−891.

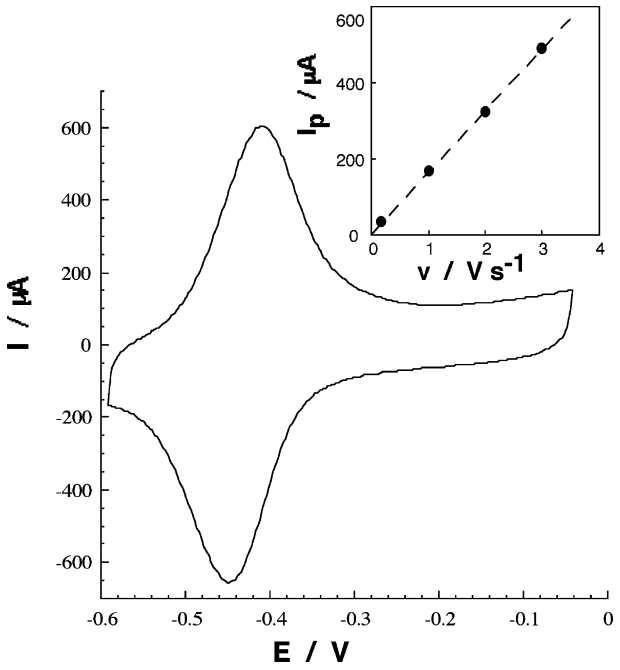

Figure 1. Cyclic voltammogram of the rotaxane-functionalized Au electrode. Potential scan rate 3 V·s^{-1}. (Inset) Peak current dependence on the potential scan rate. The data were recorded in 0.1 M phosphate buffer, pH 7.0, under Ar.

derived from the quartz-crystal microbalance (QCM) measurements performed upon assembly of the monolayer on a Au−quartz piezoelectric crystal using similar synthetic steps.

The binding properties of the electron-acceptor cyclophane (**2**) to the π-electron-donor binding sites in the molecular string structure were previously characterized in solution as well as in the monolayer configuration using absorption spectroscopy, microgravimetric quartz-crystal microbalance (QCM), and chronocoulometric measurements.[24] From these studies the association constant of **2** to the π-electron-donor binding site in the monolayer was estimated to be $K_a = 1 \times 10^4$ M^{-1}. In fact, by knowing the association constant between **2** and the binding sites, we were able to apply the optimal bulk concentration of the cyclophane (**2**) to reach a high population of the equilibrium donor−acceptor complex on the electrode surface. Upon coupling of 1-amino-adamantane stopper units with the coexisting solubilized cyclophane (**2**), the equilibrated surface structure is trapped in the rotaxane configuration.

The redox-active rotaxane monolayer was characterized by cyclic voltammetry. Figure 1 shows a cyclic voltammogram of the rotaxane-functionalized Au electrode. The quasi-reversible redox process, $E^\circ = -0.43$ V, corresponding to the redox process of the cyclophane (**2**) in the rotaxane configuration, reveals a peak-to-peak separation, ΔE_p, of 23 mV (potential scan rate 3 V·s^{-1}). The electrochemical process corresponds to the first step of the cyclophane (**2**) reduction/oxidation that includes transfer of 2e$^-$ per molecule,[22f] Scheme 1. The peak currents (cathodic and anodic) linearly increase with the increase of the potential scan rate in a large range of scan rates, Figure 1 (inset), thus indicating that the rotaxane exists as a surface-confined redox system. Coulometric analysis of the cathodic (or anodic) wave indicates a surface coverage of the redox-active cyclophane (**2**) of 0.8×10^{-10} mol·cm^{-2}, which corresponds to ca. 80% of the molecular strings formed on the electrode surface. This surface coverage translates to a surface density of the cyclophane units of ca. 0.48 molecules·nm^{-2}. Taking into account the experimental surface coverage of the cyclophane (**2**) and knowing its structural dimensions ($10 \times 13 \times 19$ Å),[29] we find that a random densely packed monolayer is formed with an approximate tilt of 40° (relative to the normal to the surface). The capacitance current of the cyclic voltammogram in the potential range from −0.05 to −0.25 V (the potential range of the ideal polarization) corresponds to the double-charged layer capacitance value of ca. 20 μF·cm^{-2}. The potential of zero charge (E_{pzc}) of the electrode was determined by following the capacitance of the modified electrode at a frequency of 100 Hz in the potential range from 0.4 to −0.25 V. The derived E_{pzc} was ca. 0.1 V.

To analyze the kinetics of the cathodic and anodic processes associated with the surface-confined redox species, we performed chronoamperometric measurements.[30] The time-dependent current, $I(t)$, generated upon reduction or oxidation of the surface-confined redox species after application of a potential step is given by eq 1a in the case of a monoexponential current decay provided by a single population of the redox component or expressed by eq 1b when a biexponential current decay originates from two different populations of the redox species

$$I(t) = k_{et} Q \cdot \exp(-k_{et} t) \quad (1a)$$

$$I(t) = k_{et1} Q_1 \cdot \exp(-k_{et1} t) + k_{et2} Q_2 \cdot \exp(-k_{et2} t) \quad (1b)$$

where k_{et} is the electron-transfer rate constant between the redox species and the electrode and Q is the charge associated with the reduction (or oxidation) of the redox species linked to the electrode surface.[31] Using eqs 1a and 1b one can derive the rate constants and charges associated with the electrochemical processes of two redox species (Q_1 and Q_2), and the respective electron transfer rate constants (k_{et1} and k_{et2}) can be found. Previous studies indicated[32] that the interfacial electron-transfer rate constant is controlled by the distance separating the redox unit and the electrode surface. Indeed, several studies[22c,33] have analyzed the dynamics of structural changes of redox-active components associated with electrodes by following the electron-transfer rate constants at the conductive supports.

We applied chronoamperometry to follow the dynamics of shuttling of cyclophane (**2**) on the functional molecular wire. Figure 2A shows the current transient observed upon application of a reductive potential step on the rotaxane-functionalized electrode from −0.33 to −0.53 V after prebiasing of the electrode at −0.33 V for 10 s. Under these conditions the cyclophane (**2**) initially exists in its oxidized state, and upon application of the potential step it is reduced to the respective biradical, Scheme 1. Kinetic analysis, Figure 2A (inset), of the current transient indicates a monoexponential interfacial electron-transfer process with a rate constant that corresponds to $k_{et} = 80$ s^{-1}. The single exponent observed for the current transient

(29) Ashton, P. R.; Odell, B.; Reddington, M. V.; Slawin, A. M. Z.; Stoddart, J. F.; Williams, D. J. *Angew. Chem., Int. Ed. Engl.* **1988**, *27*, 1550−1553.
(30) (a) Finklea, H. O.; Ravenscroft, M. S.; Snider, D. A. *Langmuir* **1993**, *9*, 223−227. (b) Chidsey, C. E. D. *Science* **199**1, *251*, 919−922. (c) Katz, E.; Itzhak, N.; Willner, I. *Langmuir* **1993**, *9*, 1392−1396.
(31) (a) Forster, R. J.; Faulkner, L. R. *Anal. Chem.* **1995**, *67*, 1232−1239. (b) Forster, R. J. *Langmuir* **1995**, *11*, 2247−2255. (c) Forster, R. J. *Anal. Chem.* **1996**, *68*, 3143−3150. (d) Forster, R. J. *Analyst* **1996**, *121*, 733−741.
(32) Katz, E.; Willner, I. *Langmuir* **1997**, *13*, 3364−3373.
(33) Pardo-Yissar, V.; Katz, E.; Willner, I.; Kotlyar, A. B.; Sanders, C.; Lill, H. *Faraday Discuss.* **2000**, *116*, 119−134.

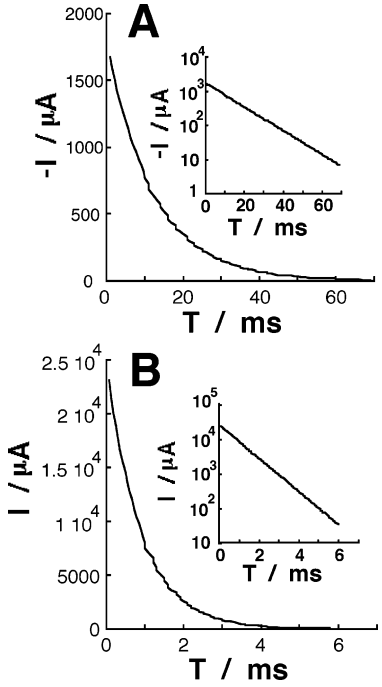

Figure 2. (A) Current transient observed upon application of a potential step from −0.33 to −0.53 V on the rotaxane-functionalized Au electrode that was prebiased at −0.33 V for 10 s. (Inset) Kinetic analysis of the current transient curve. (B) Current transient observed upon application of a potential step from −0.53 to −0.33 V on the rotaxane-functionalized Au electrode that was prebiased at −0.53 V for 10 s. (Inset) Kinetic analysis of the current transient curve. All data were recorded in 0.1 M phosphate buffer, pH 7.0, under Ar.

indicates that the cyclophane (**2**) exists in a single configuration on the molecular string (vide infra for further discussion). Figure 2B shows the current transient observed upon application of an oxidative potential step on the rotaxane-functionalized electrode from −0.53 to −0.33 V after prebiasing of the electrode at −0.53 V for 10 s. Under these conditions the cyclophane (**2**) initially exists in its reduced state and its oxidation proceeds upon applying the potential step. The current transient follows monoexponential kinetics, Figure 2B (inset), and the derived rate constant corresponds to $k_{et} = 1100\ s^{-1}$. The surface coverage of the redox units associated with the electrodes was calculated using eq 1a from the preexponential factors and the respective rate constants upon analyzing the cathodic and anodic current transients, yielding a value of ca. 0.8×10^{-10} mol·cm^2, which is similar to that derived from cyclic voltammetry. Thus, oxidation of the reduced cyclophane proceeds with a substantially higher electron-transfer rate constant as compared to the reduction process. These results are explained by the fact that the oxidized cyclophane (**2**) is localized on the π-donor site by π-donor/acceptor interactions (even though the electrode is negatively charged), and the spatial distance separation of the redox-active cyclophane (**2**) from the electrode results in the slow electron-transfer rate. Reduction of the cyclophane unit depletes the electron-acceptor properties, resulting in dissociation of the supramolecular complex on the molecule string. Since the electrode is negatively charged, the positively charged reduced cyclophane is attracted by the electrode, and the resulting short distance with respect to the electrode leads to fast electron transfer upon oxidation of the reduced cyclophane, Scheme 1.

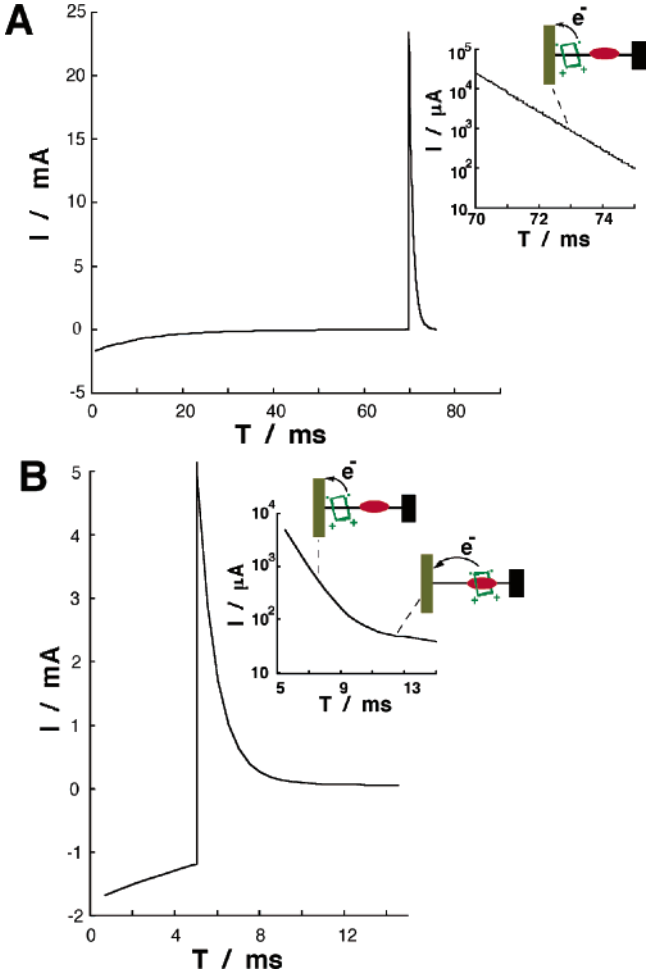

Figure 3. Double-potential step chronoamperometric experiments on the rotaxane-monolayer electrode where the electrode was prebiased at −0.33 V for 10 s, then the potential was stepped from −0.33 to −0.53 V followed by the potential stepping from −0.53 to −0.33 V: (A) time interval of the first potential step is 70 ms and (B) time interval of the first potential step is 5 ms. (Insets) Anodic current decays upon the second potential step shown in a semilogarithmic form. All data were recorded in 0.1 M phosphate buffer, pH 7.0, under Ar.

The chronoamperometric experiments allowed us to identify a molecular mechanical translocation of cyclophane (**2**) on the molecular string and enabled us to characterize the positions of the oxidized or reduced cyclophane in the dynamic process. A major challenge in characterizing molecular mechanical translocation is, however, determination of the speeds of the translocation on the molecular string. This aspect was studied by applying double-potential step chronoamperometric experiments on the system in its different configurations. At first the rotaxane-monolayer electrode was biased at a potential of −0.33 V for 10 s to generate the oxidized state of the cyclophane (**2**) associated with the π-electron-donating site. Then, a potential step from −0.33 to −0.53 V was applied for 70 ms to yield the fully reduced cyclophane, and a second potential step from −0.53 V to −0.33 V was applied to reoxidize the reduced cyclophane. Figure 3A shows the transient current upon this double-potential step experiment. The cathodic current transient observed upon the first negative potential step shows the slow electron-transfer kinetics (rate constant ca. 80 s^{-1}) characteristic of the long-distance electron transfer to the cyclophane units associated with the π-donor binding site. However, the reversed anodic current transient observed after 70 ms reveals the fast

monoexponential decay (rate constant ca. 1100 s^{-1}, Figure 3A (inset)) characteristic of the electron transfer between the reduced cyclophane positioned close to the electrode surface. Thus, a time interval of 70 ms between the initiation of the cyclophane reduction and its reoxidation is long enough to allow the complete translocation of the reduced cyclophane from the π-donor binding site to the electrode surface. To find the reduced cyclophane units still on the π-donor binding sites and eliminate their complete translocation to the electrode surface, the time interval between the cathodic and anodic steps should be shortened. Nonetheless, one should realize that since the electron transfer to the cyclophane bound to the π-donor is slow, only a fraction of the cyclophane units could be reduced upon application of the reductive potential for time intervals shorter than 70 ms. Figure 3B shows the current transients observed when the reduction process at −0.53 V proceeds for 5 ms (resulting in reduction of ca. 26% of the cyclophane), and then the potential step is reversed to −0.33 V. The anodic current decay corresponding to reoxidation of the reduced cyclophane shows biexponential time dependence, Figure 3B (inset), that consists of a fast component of the current decay with a rate constant of ca. 1100 s^{-1} and a slow current decay component exhibiting a rate constant of ca. 80 s^{-1}. The rate constants and the respective populations of the cyclophane were derived from the experimental current transients using eq 1b. The fast anodic current decay that corresponds to ca. 80% of the reduced cyclophane generated during the 5 ms time interval of the cathodic process is attributed to oxidation of a population of the reduced cyclophane that is close to the electrode surface. On the other hand, the slow anodic current transient is attributed to the oxidation of a population of the reduced cyclophane (ca. 20% of the reduced product) that is still associated with the π-donor binding site. This experiment clearly indicates that by application of a double-potential step chronoamperometric experiment with an appropriate time gap between the pulses, we may identify two populations of the reduced cyclophane. One fraction, which escaped the original π-donor binding site, was translocated toward the electrode surface, Scheme 1, whereas another fraction of the reduced cyclophane is still bound to the original binding site.

The opposite translocation of the cyclophane from the electrode surface to the π-donor binding site was also studied using the double-potential step chronoamperometric method. At first, the rotaxane-monolayer-modified electrode was biased at −0.53 V for 10 s to yield the reduced state of the cyclophane that is concentrated near the electrode surface. Then a positive potential step from −0.53 to −0.33 V was applied, resulting in a fast anodic current transient (rate constant ca. 1100 s^{-1}), yielding the fully oxidized cyclophane within 5 ms. The opposite potential step, from −0.33 to −0.53 V, resulting in reduction of the cyclophane (**2**) was applied after different time intervals of 5, 50, and 100 ms, Figure 4A, B, and C, respectively. Upon the electrochemical oxidation of the cyclophane (**2**) its translocation from the electrode surface to the π-donor binding site is initiated, and different populations of the oxidized cyclophane at the electrode surface and at the binding site are anticipated to be identified as a function of the time gap separating the oxidation and reduction steps. The fast monoexponential cathodic current decay (the rate constant ca. 1100 s^{-1}) is observed with a time gap of 5 ms, Figure 4A (inset), indicating

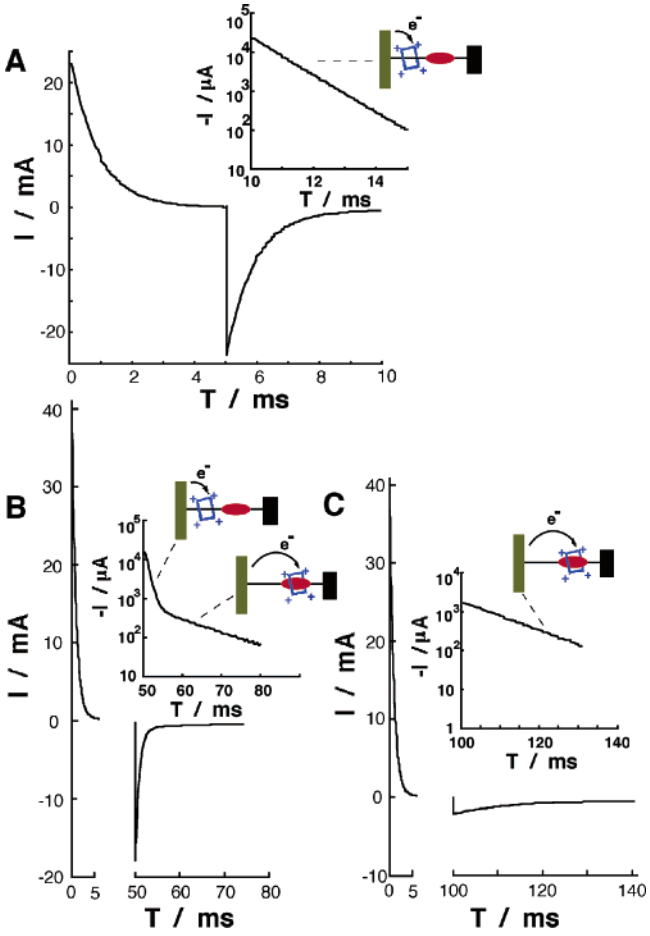

Figure 4. Double-potential step chronoamperometric experiments on the rotaxane-monolayer electrode where the electrode was prebiased at −0.53 V for 10 s, then the potential was stepped from −0.53 to −0.33 V followed by the potential stepping from −0.33 to −0.53 V: (A) time interval of the first potential step is 5 ms, (B) time interval of the first potential step is 50 ms, and (C) time interval of the first potential step is 100 ms. (Insets) Cathodic current decays upon the second potential step shown in a semilogarithmic form. All data were recorded in 0.1 M phosphate buffer, pH 7.0, under Ar.

that the oxidized cyclophane is still close to the electrode surface. The biexponential current decay composed of the fast and slow components (ca. 1100 s^{-1}, ca. 63% of the cyclophane and ca. 80 s^{-1}, ca. 37% of the cyclophane, respectively, derived using eq 1b) is observed with a time gap of 50 ms, Figure 4B (inset). This implies that ca. 63% of the oxidized cyclophane is still near the electrode surface, whereas ca. 37% of the oxidized cyclophane is already associated with the binding site. With a time gap of 100 ms the cathodic current shows only slow monoexponential decay (the rate constant ca. 80 s^{-1}), revealing that all cyclophane units moved to the π-donor binding site. Knowing the populations of the cyclophane in the two positions (close to the electrode surface and on the π-donor binding site) upon moving in the two defined directions, we estimated the first-order rate constants associated with the motion of the cyclophane along the molecular string. The electrochemically driven redox shuttle moves from the π-donor binding site to the electrode surface with a first-order rate constant $k_1 = 320$ s^{-1} (fast process), whereas the cyclophane movement from the electrode surface to the π-donor binding site proceeds with slower kinetics, $k_2 = 9.2$ s^{-1}. The difference in the rate constants of the molecule translocation is attributed to directional

electrostatic force acting on the moving cyclophane. In both reduced and oxidized states the cyclophane is positively charged (+2 and +4, respectively), while the applied potentials (−0.53 or −0.33 V) provide a negatively charged conductive support. Thus, translocation of the reduced cyclophane, which lacks affinity to the π-donor binding site, to the electrode surface is assisted by the electrostatic attraction to the electrode surface, resulting in the fast process. On the moving of the oxidized cyclophane from the electrode surface, it should overcome this electrostatic force resulting in the slow process. Thus, translocation of the oxidized cyclophane (**2**) on the molecular string is a thermally activated process that is "braked" by its competitive electrostatic attraction by the electrode. Once the cyclophane reaches the π-donor binding site, a stable donor−acceptor complex is formed. This essentially traps the cyclophane on the molecular string, and its electrostatic attraction by the electrode cannot overcome the supramolecular complex stabilization. It should be noted, however, that the speed of the mechanic translocation of the threaded cyclophane is comparable with the electron-transfer process used to follow the cyclophane movement, and thus, the derived values of the rate constants represent only approximate values.

Translocation of the cyclophane units along the molecular strings upon reduction/oxidation processes suggests that the interfacial properties, such as electrical capacitance and wettability of the electrode surface, should be controlled by the oxidation state of the cyclophane and electrochemically switched upon changing the potential applied on the electrode. To study the electrical interfacial properties of the system we performed impedance spectroscopy studies on the functionalized electrode. Impedance spectroscopy is a powerful method to characterize the electrical interfacial properties,[34] and it was applied in many sensing and biosensing systems as a transduction technique.[35] The theoretical background of impedance spectroscopy for the surface-confined redox species was developed by Laviron.[36] Several systems, including redox species chemically bound to electrode surfaces or strongly adsorbed on electrode surfaces, were studied using impedance spectroscopy.[37] Use of impedance spectroscopy to characterize surface-confined redox processes did not develop, however, to a routine technique, and a basic theoretical introduction is needed prior to discussion of the experimental results.

Upon application of an appropriate potential on an electrode immersed in a solution that includes a redox species, a steady-state direct current (DC) corresponding to the reduction or oxidation of the redox component is generated. For a system consisting of a surface-confined redox species, a steady-state direct current cannot be supported due to the limited amount of the electroactive component, and application of a potential step on the electrode results in a transient current decay observed by chronoamperometry. This results in transition from the reduced to the oxidized state or from the oxidized to the reduced state of the redox component, and after the surface-confined system reaches equilibrium at a new potential, the current equals to zero. This difference between solution and surface-confined redox species is also reflected by the electrochemical impedance spectroscopy. The complex impedance can be presented as the sum of the real, $Z_{re}(\omega)$, and imaginary, $Z_{im}(\omega)$, components originating mainly from the resistance and capacitance of the cell, respectively, measured at a variable circular frequency ω. Experimental Faradaic impedance spectra obtained for a bulk solution consisting of a redox species can be fitted by computer simulation using an equivalent electronic circuit based on the Randles and Ershler theoretical model.[34,38] This equivalent circuit includes the ohmic resistance of the electrolyte solution, R_s, the Warburg impedance, Z_W, resulting from diffusion of the redox probe, the double-layer capacitance, C_{dl}, and the electron-transfer resistance, R_{et}, Scheme 2A. A typical shape of a Faradaic impedance spectrum obtained for a solution of a redox species (presented in the form of a Nyquist plot) includes a semicircle region lying on the Z_{re} axis followed by a straight line, Scheme 2B. The semicircle portion, observed at higher frequencies, corresponds to the electron-transfer-limited process, whereas the linear part of the spectrum is characteristic of the lower frequency range and represents the diffusion-limited electrochemical process. The semicircle diameter in the impedance spectrum equals the electron-transfer resistance, R_{et}. When applying impedance spectroscopy to a surface-confined redox system the experimental spectra can be fitted using the equivalent circuit shown in Scheme 2C. The equivalent circuit includes the ohmic resistance of the electrolyte solution, R_s, the double-layer capacitance, C_{dl}, the electron-transfer resistance, R_{et}, and the pseudocapacitance, C_{pc}, corresponding to the electrochemical charging/discharging process of the surface-confined redox species.[37a] The obvious difference between the equivalent circuits for the diffusional and surface-confined redox species systems (Scheme 2A and C, respectively) is that the former circuit is conductive for the direct current (or low-frequency alternative current) whereas the later circuit is not. This is consistent with the fact that surface-confined redox systems do not support steady-state direct current. The electrochemical impedance spectra for surface-confined redox systems are usually presented in the form of Cole−Cole plots, particularly in the form of C_{im} vs C_{re} (where C_{im} and C_{re} are imaginary and real parts of the interfacial complex capacitance, respectively).[34] The Cole−Cole presentation describes the distribution of relaxation processes corresponding to the charging of the monolayer. The complex capacitance used in this work is the same as the frequency normalized complex admittance $Y\omega^{-1}$ that is proportional to the complex permittivity.[34c] Thus, the imaginary and real parts of the capacitance (C_{im} and C_{re}) could be also described in terms of the imaginary and real parts of the impedance Z, eqs 2 and 3

$$C_{im} = -Im[(j\omega Z)^{-1}] \quad (2)$$

$$C_{re} = Re[(j\omega Z)^{-1}] \quad (3)$$

The typical shape of this plot corresponds to a semicircle lying

(34) (a) Bard, A. J.; Faulkner, L. R. *Electrochemical Methods: Fundamentals and Applications*; Wiley: New York, 1980. (b) Stoynov, Z. B.; Grafov, B. M.; Savova-Stoynova, B. S.; Elkin, V.V. *Electrochemical Impedance*; Nauka: Moscow, 1991. (c) *Impedance Spectroscopy;* Macdonalds, J. R., Ed.; Wiley-Interscience: New York, 1987.
(35) Katz, E.; Willner, I. *Electroanalysis* **2003**, *15*, 913−947.
(36) (a) Laviron, E. *J. Electroanal. Chem.* **1979**, *105*, 35−42. (b) Lelievre D.; Plichon, V.; Laviron, E. *J. Electroanal. Chem.* **1980**, *112*, 137−145.
(37) (a) Nahir, T. M.; Bowden, E. F. *Langmuir* **2002**, *18*, 5283−5286. (b) Sagara, T.; Niwa, K.; Sone, A.; Hinnen, C.; Niki, K. *Langmuir* **1990**, *6*, 254−262. (c) Ataka, K.; Hara, Y.; Osawa, M. *J. Electroanal. Chem.* **1999**, *473*, 34−42. (d) Creager, S. E.; Wooster, T. T. *Anal. Chem.* **1998**, *70*, 4257−4263. (e) Song, S.; Clark, R. A.; Bowden, E. F.; Tarlov, M. J. *J. Phys. Chem.* **1993**, *97*, 6564−6572.
(38) (a) Randles, J. E. B. *Discuss. Faraday Soc.* **1947**, *1*, 11−19. (b) Ershler, B. V. *Discuss. Faraday Soc.* **1947**, *1*, 269−277.

Scheme 2 [a]

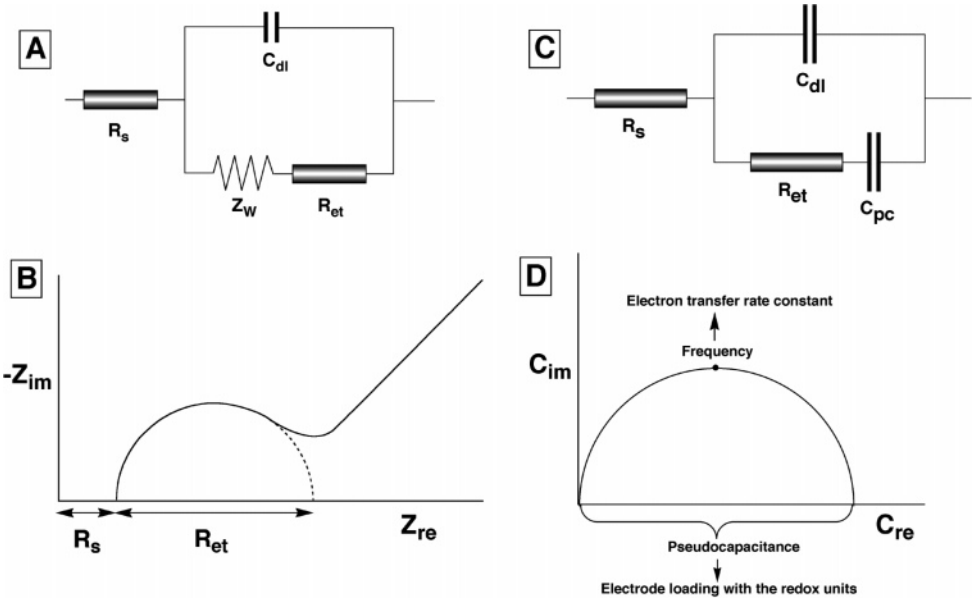

[a] (A) Equivalent circuit for a Faradaic impedance spectrum measured in the presence of a diffusional redox probe (Randles and Ershler theoretical model). (B) Typical shape of an impedance spectrum in the presence of a diffusional redox probe (Nyquist plot). (C) Equivalent circuit for a Faradaic impedance spectrum corresponding to a surface-confined redox species on an electrode. (D) Typical shape of an impedance spectrum in the presence of surface-confined redox species (Cole−Cole plot).

on the C_{re} axis (assuming, for simplicity, that the pseudocapacitance, C_{pc}, is much bigger than the double-layer capacitance, C_{dl}). The diameter of this semicircle corresponds to the pseudocapacitance value, C_{pc}. The surface concentration of the redox-active surface-confined species, Γ, could be derived from the pseudocapacitance value, C_{pc}, using eq 4[36b,37a]

$$\Gamma = 4RTC_{pc}(nF)^{-2}A^{-1} \quad (4)$$

where R is the universal gas constant, T is the temperature, F is the Faraday constant, n is the number of electrons per molecule participating in the electrochemical reaction, and A is the electrode surface area. Another important parameter of the surface-confined redox system is the rate constant of the electron-transfer process, k_{et}. This rate constant could be derived from the frequency, f°, corresponding to the maximum value of the imaginary capacitance, C_{im}^{max}, using eq 5.[37a]

$$k_{et} = \pi f^{\circ} \quad (5)$$

Thus, the surface concentration of the surface-confined redox species and the electron-transfer rate constant could be derived from a single impedance spectrum.

Figure 5A shows the impedance spectrum composed of two semicircles obtained upon application of the potential equal to −0.33 V to the modified electrode, where the redox cyclophane (**2**) exists in the oxidized state. The small semicircle observed at high frequencies could be also observed when the redox cyclophane is excluded from the monolayer, whereas the big semicircle appears only if the system includes the redox component. Thus, the small semicircle corresponds to the double-layer capacitance, C_{dl}, of the monolayer, whereas the large semicircle originates from the electron-transfer process between the conductive support and the surface-confined redox species (pseudocapacitance, C_{pc}). Computer fitting of the experimental spectrum using the equivalent circuit shown in

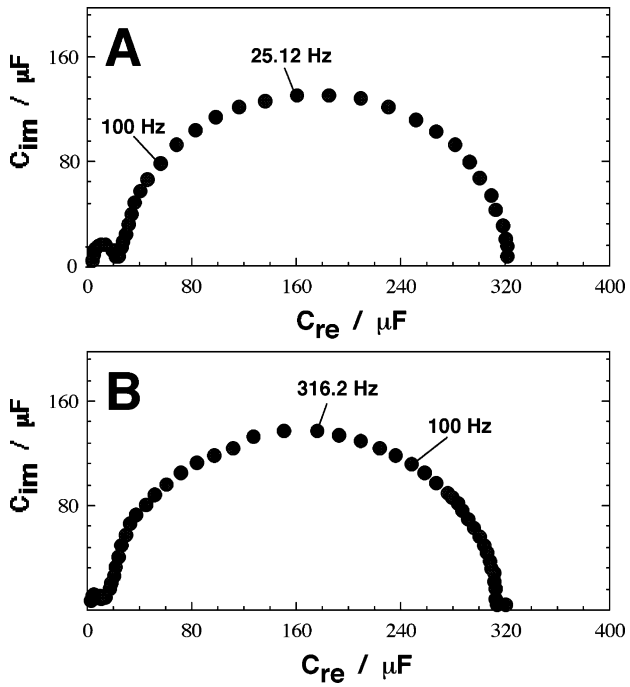

Figure 5. Impedance spectra corresponding to the rotaxane-functionalized Au electrode in the form of Cole−Cole plots obtained at different biasing potentials: (A) $E_{bias} = -0.33$ V, (B) $E_{bias} = -0.53$ V. All data were recorded in 0.1 M phosphate buffer, pH 7.0, under Ar.

Scheme 2C yields $C_{dl} = 25\ \mu$F and $C_{pc} = 300\ \mu$F. It should be noted that the C_{dl} value derived from the impedance measurements is similar to that observed by the cyclic voltammetry in the potential range of −0.05 to −0.25, where the cyclophane (**2**) exists in the oxidized state. The surface coverage of the redox cyclophane (**2**) was derived from C_{pc} using eq 4 to be ca. 0.8 $\times\ 10^{-10}$ mol·cm^{-2}, a value similar to that obtained from the cyclic voltammetry or chronoamperometry measurements. The electron-transfer rate constant, k_{et}, ca. 77 s^{-1}, was estimated from

the frequency corresponding to the maximum value of C_{im} and using eq 5. This value is very close to the electron-transfer rate constant derived from the chronoamperometry experiments ($k_{et} = 80\ s^{-1}$). Figure 5B shows the impedance spectrum obtained upon application of the potential equal to −0.53 V on the modified electrode, where the redox cyclophane (**2**) exists in the reduced state. The impedance spectrum is composed of very small semicircle corresponding to the double-layer capacitance ($C_{dl} = 12\ \mu F$) and a large semicircle similar to that observed in Figure 5A ($C_{pc} = 300\ \mu F$) but appearing at higher frequencies. Application of eqs 4 and 5 to the large semicircle results in the same surface coverage of the redox cyclophane, $\Gamma = 0.8 \times 10^{-10}$ mol·cm^{-2}, but the derived electron-transfer rate constant is $k_{et} = 1080\ s^{-1}$, a value that is substantially higher than that observed for the oxidized cyclophane (**2**). The calculated value for the interfacial electron-transfer rate constant is similar to the value derived from the chronoamperometric measurements, $k_{et} = 1100\ s^{-1}$. The higher rate constant observed for the electron transfer between the reduced cyclophane and the conductive support originates from the fact that the reduced cyclophane is dissociated from the π-electron-donor site and attracted to the electrode surface by electrostatic interaction, thus providing the short distance for the electron transfer. The lower rate constant observed for the electron transfer between the conductive support and the oxidized cyclophane corresponds to the long-distance electron transfer to the remote position of the cyclophane (**2**) associated with the π-electron-donor site. The different kinetics of the electron transfer[39] at different applied potentials results in the appearance of the pseudocapacitance semicircles at different frequencies (higher frequencies at the reductive potential and lower frequencies at the oxidative potential). Thus, the C_{re} value measured at a fixed frequency depends on the redox state of the system controlled by the applied potential. Figure 6 shows the switching of the C_{re} at 100 Hz between two values of ca. 57 and ca. 247 μF upon changing the applied potential between two values of −0.33 and −0.53 V, respectively.

It should be noted that the chronoamperometric measurements and impedance experiments represent quite different methods: while chronoamperometry involves a high-magnitude potential perturbation, the impedance measurements include a low-magnitude perturbation in the system. Nonetheless, the derived interfacial electron-transfer rate constants are very similar despite the different techniques. We also emphasize that the derived electron-transfer rate constants should be considered as apparent rate constants, and their values are higher than the standard electron-transfer rate constants corresponding to the reaction at $E°$ since we apply overpotentials (±100 mV vs $E°$) in our experiments (chronoamperometry as well as impedance spectroscopy). Nevertheless, it should be noted that the apparent rate constants (corresponding to the slow and fast components) are almost indistinguishable in the oxidative or reductive steps, implying that the overpotentials and the Frumkin effect have a small contribution to the electron-transfer constants.

(39) The kinetic nonsymmetricity of the reduction/oxidation process was also observed by cyclic voltammetry. The cathodic peak demonstrates a much larger shift than the anodic peak upon potential scan increase provided that the cathodic process is slower than the anodic reaction. The experimental results and detailed discussion are given in the Supporting Information.

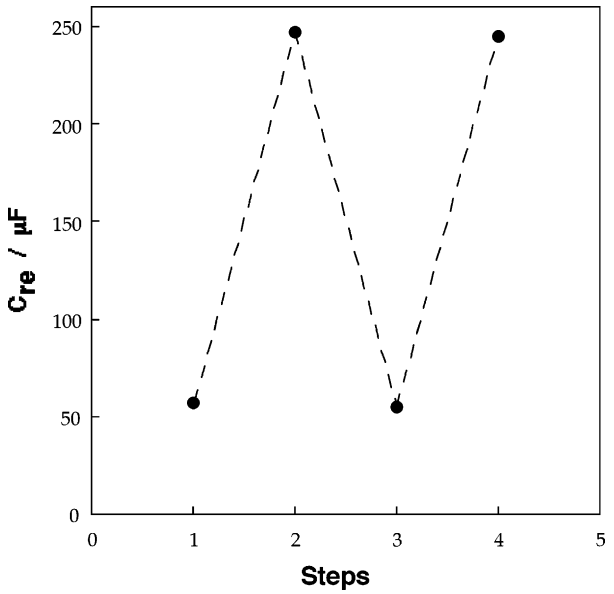

Figure 6. Reversible switching of the real capacitance, C_{re}, measured at the frequency of 100 Hz upon the cyclic change of the bias potential on the electrode: Steps 1 and 3 were measured at $E_{bias} = -0.33$ V, steps 2 and 4 were measured at $E_{bias} = -0.53$ V. The C_{re} values were derived from the impedance spectra shown in Figure 5.

Translocation of the redox cyclophane units is based on the different affinities of the oxidized and reduced cyclophane units for the diiminobenzene π-electron-donor sites on the molecular strings. Protonation of the diiminobenzene units should, however, deplete the electron-donating properties of these components and eliminate the binding sites for the cyclophane units. Thus, one could expect that translocation of the redox cyclophane units upon reduction/oxidation will not be possible when the diiminobenzene sites are protonated. Accordingly, to gain further support for the molecular mechanical translocation we characterized the function of the system at different pH values. The acidic/basic equilibrium at various self-assembled monolayers has been studied using different methods,[40] including impedance spectroscopy.[41] The interfacial properties of the electrode modified with the molecular strings in the absence of the cyclophane units were probed at various pH values by Faradaic impedance spectroscopy in the presence of $[Fe(CN)_6]^{3-/4-}$ as redox label, Scheme 3. Electron transfer to the negatively charged redox label is anticipated to be facilitated in the presence of the protonated monolayer due to the electrostatic attraction of the redox species.[41] As a result, the interfacial electron-transfer resistance in the system that includes the protonated monolayer, $R_{et'}$, should be smaller than the electron-transfer resistance in the presence of the nonprotonated monolayer, $R_{et''}$, Scheme 3A and B.

Figure 7A, curve a, shows the impedance spectrum (in the form of a Nyquist plot) corresponding to the monolayer-functionalized electrode at pH = 7.0, where the monolayer is assumed to be in the nonprotonated neutral state. Computer fitting of the experimental impedance spectrum using the

(40) (a) Kane, V.; Mulvaney, P. *Langmuir* **1998**, *14*, 3303−3311. (b) Fawcett, W. R.; Fedurco, M.; Kovacova, Z. *Langmuir* **1994**, *10*, 2403−2408. (c) Bryant, M. A.; Crooks, R. M. *Langmuir* **1993**, *9*, 385−387. (d) Zhao, J.; Luo, L.; Yang, X.; Wang, E.; Dong, S. *Electroanalysis* **1999**, *11*, 1108−1111. (e) Creager, S. E.; Clarke, J. *Langmuir* **1994**, *10*, 3675−3683.

(41) (a) Komura, T.; Yamaguchi, T.; Shimatani, H.; Okushio, R. *Electrochim. Acta* **2004**, *49*, 597−606. (b) Schweiss, R.; Werner, C.; Knoll, W. *J. Electroanal Chem.* **2003**, *540*, 145−151.

Scheme 3. Electron-Transfer Processes of a Negatively Charged Diffusional Redox Probe across the Monolayer on the Electrode Surface[a]

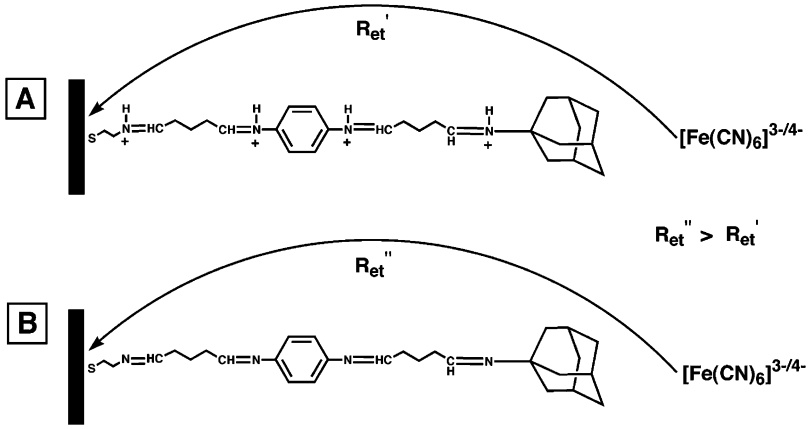

[a] (A) The protonated molecular strings in the monolayer. (B) The nonprotonated molecular strings in the monolayer. $R_{et'}$ and $R_{et''}$ represent the respective electron-transfer resistances.

Randles and Ershler equivalent circuit outlined in Scheme 2A yields the electron-transfer resistance value of $R_{et''} = 19.6$ kΩ. A smaller electron-transfer resistance, $R_{et'} = 10.1$ kΩ, is derived from the impedance spectrum obtained at pH = 2.1, Figure 7A, curve b. In the later system, the monolayer exists in its protonated state, which facilitates electron transfer by electrostatic attraction of the redox label. The Faradaic impedance measurements performed at various pH values provided the electron-transfer resistances, which were plotted as a function of pH, yielding the respective titration curve, Figure 7B. The pK_a of the monolayer that is derived from the titration curve corresponds to ca. 4.2. Thus, we could expect that the molecular strings and, particularly, the diiminobenzene units exist in the protonated state at pH = 2.0, whereas at pH > 6 the monolayer is present in a nonprotonated state. It should be noted that the monolayer might be ruined at the acidic conditions of the later experiment due to the acid-catalyzed dissociation of the Schiff-base bonds present in the molecular strings.[42] Although some protonated Schiff bases appear to be relatively stable, particularly when incorporated in membranes (e.g., rhodopsin),[43] the stability of the monolayer is important for interpretation of our results, since the observed decrease in the electron-transfer resistance upon acidification of the solution may also originate from degradation of the monolayer. The stability of the monolayer composed of the molecular strings and the threaded redox-active cyclophane was studied by cyclic voltammetry at pH = 7.0, 4.0, and 2.0, Figure 8, curves a, b, and c, respectively. In these experiments the surface coverage of the threaded cyclophane was followed by cyclic voltammetry as a function of time in the different aqueous solutions. One can see that the monolayers exposed to the neutral solution, pH = 7.0, and the slightly acidic solution, pH = 4.0, are rather stable during the period of measurements (3 h), whereas the monolayer reveals lower stability in the strong acidic solution, pH = 2.0, (ca. 2%, 4%, and 56% decrease in the surface coverage of the cyclophane is observed within 3 h at pH = 7.0, 4.0, and 2.0, respectively). It should be noted, however, that the monolayer-modified electrode, on which the impedance measurements outlined in Figure 7 were performed, was exposed to acidic solutions (pH range from 4.0 to 2.0) for less than 30 min, and the impedance spectrum at pH = 2.0 was measured for less than 10 min. Thus, during this time interval the monolayer electrode is relatively stable at acidic conditions, and any electrochemical measurements on the interface may assume the intact structure of the monolayer. Finally, to prove that the modified electrode has survived after the impedance measurements in acidic medium, we recorded the cyclic voltammogram and found that only ca. 5% of its original activity has disappeared. These stability measurements confirm that the change of the impedance spectra upon varying the pH value of the solution originate from the acid/base equilibrium at the monolayer interface rather than its chemical instability. Also, after completion of the impedance measurements at pH = 2.0 that showed the low electron-transfer resistance, the impedance measurements were reconducted on the same electrode at pH = 7.0, and this resulted in ca. 93% of the high-electron-transfer resistance value, indicating that the impedance changes are reversible.

Chronoamperometric measurements, similar to those outlined in Figure 2, were performed at different pH values between pH = 7.0 and 2.0 by applying a potential step from $E = -0.33$ to -0.55 V (the reductive potential step) and following the resulting cathodic current transients. The current transients (in a semilogarithmic plot) are shown in Figure 9A. One may see that the current decay observed at pH = 7.0, Figure 9A, curve a, corresponds to the slow monoexponential kinetics similar to that shown in Figure 2A. This is consistent with the location of the cyclophane in the remote position on the π-donor binding site. At pH = 2, where the diiminobenzene sites are protonated and lose their π-donor properties, only fast electron-transfer kinetics is observed, Figure 9A, curve e. This is consistent with the fact that under these conditions the cyclophane is not linked to the protonated diiminobenzene sites and is attracted by the electrostatic interactions to the electrode surface. The close distance between the cyclophane and the electrode surface results in the fast cathodic current transient. The current transients observed upon gradual acidification of the system from pH = 5 to 4 are depicted in Figure 9A, curves b−d. Within this pH region the electron-transfer kinetics reveal a biexponential process, eq 1b,[31,32] which includes the slow electron-transfer kinetics (associated with reduction of the cyclophane bound to the nonprotonated π-donor sites) and the fast electron transfer (associated with the reduction of the cyclophane close

(42) Streitwieser, A.; Heathcock, C. H. *Introduction to Organic Chemistry*; Macmillan Publishing Co., Inc.: New York, 1976.
(43) (a) Gorostidi, G. R. E.; Santos, J. G.; Basagoitia, A.; Castillo, M.; Blanco, F. G. *Bull. Chem. Soc. Jpn.* **2003**, *76*, 335−340. (b) Yamada, A.; Kakitani, T.; Yamamoto, S.; Yamato, T. *Chem. Phys. Lett.* **2002**, *366*, 670−675.

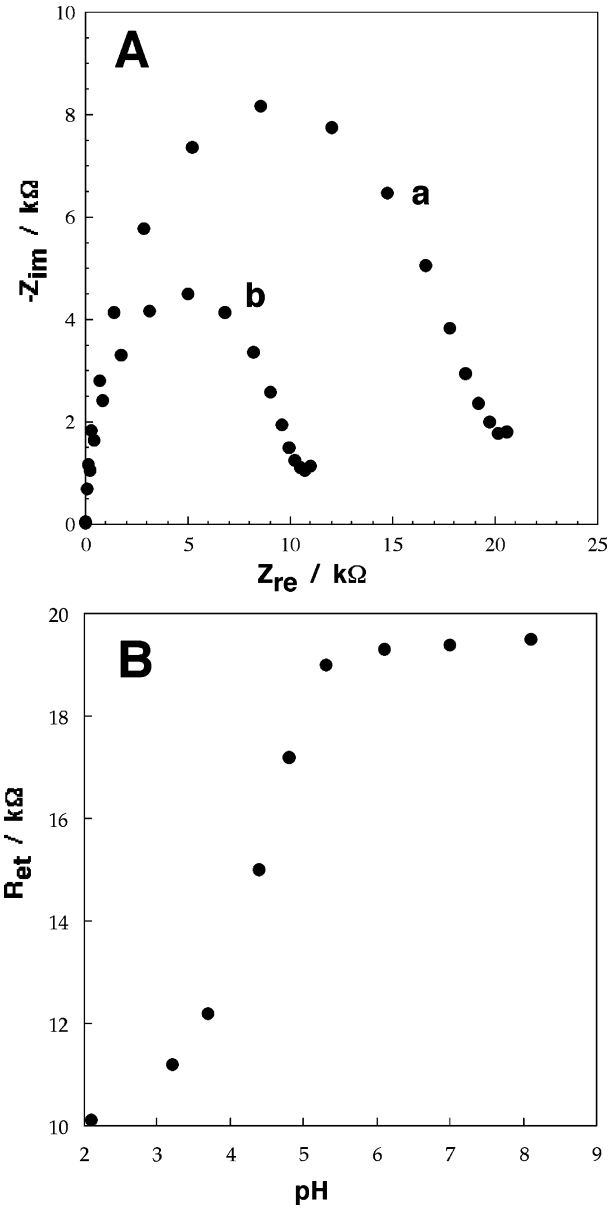

Figure 7. (A) Faradaic impedance spectra (Nyquist plots) for the modified Au electrode lacking the redox cyclophane (**2**) measured in the presence of 10 mM $K_3[Fe(CN)_6]/K_4[Fe(CN)_6]$, 1:1 mixture, at different pH values: (a) pH = 7.0, (b) pH = 2.0. (B) Electron-transfer resistances derived from the impedance spectra measured at variable pH values in the presence of the $K_3[Fe(CN)_6]/K_4[Fe(CN)_6]$ redox probe. All data were recorded under Ar in 0.1 M Britton−Robinson titrated to the different pH values and upon application of the bias potential of 0.17 V.

to the electrode surface). As the acidity of the medium increases, the fast component in the cathodic transient decay is higher and the slow component is lower. This is consistent with the fact that at higher acidities the population of the protonated diiminobenzene sites is higher, resulting in an increased population of the cyclophane at the electrode surface. Using eq 1b one may calculate the populations of the cyclophane at the different states on the molecular string for each pH value. These populations plotted as a function of pH, Figure 9B, represent the titration curves of the functional monolayer with the pK_a value of ca. 4.5 that is similar to that observed by the Faradaic impedance spectroscopy.

Electrochemical reduction/oxidation of the cyclophane (**2**) and the resulting translocation of the cyclophane along the molecule

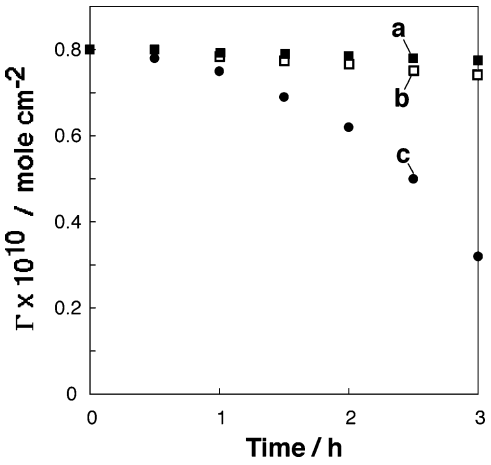

Figure 8. Stability of the rotaxane-functionalized electrode measured by cyclic voltammetry at different pH values: (a) pH = 7.0; (b) pH = 4.0; (c) pH = 2.0. All data were recorded under Ar in 0.1 M Britton−Robinson titrated to the different pH values. Potential scan rate, 3 V s^{-1}.

string are anticipated to alter the dielectric properties of the monolayer. That is, reduction of the cyclophane (**2**) results in translocation of the reduced biradical dication toward the electrode surface, a process that exposes the hydrophobic brush of the molecular strings toward the solution. This process, together with the fact that the reduction process transforms the hydrophilic tetracationic cyclophane (**2**) into a biradical dication of substantially lower hydrophilicity, implies that upon reduction of the cyclophane, the interface alters its dielectric properties and exhibits higher hydrophobicity. This should also result in the decrease of the double-charged layer capacitance, C_{dl}.[44] On the other hand, application of the oxidative potential of −0.33 V results in translocation of the oxidized cyclophane from the electrode surface to the π-donor binding site. This process would expose the hydrophilic tetracationic cyclophane (**2**) toward the solution and shield the hydrophobic contribution of the molecular strings. This also results in the increase of the double-charged layer capacitance, C_{dl}, and the increase of the hydrophilic properties of the interface. The expected changes of the double-charged layer capacitance values, C_{dl}, were observed in the impedance spectra that showed C_{dl} values of ca. 25 and ca. 12 $\mu F \cdot cm^{-2}$ for potentials of −0.33 and −0.53 V, respectively, Figure 5. Electrochemical control of the hydrophilic/hydrophobic properties of monolayer-modified surfaces has been studied by in situ electrochemical/contact angle measurements.[45] For example, electrical bending of carboxylate-terminated long-chain alkane thiols[45a] or the structural bending of long-chain alkane thiols modified with redox-active headgroups[45b] were used to control the hydrophilic/hydrophobic properties of Au-coated surfaces. The corresponding changes of the hydrophobic/hydrophilic properties of the rotaxane-modified interface where studied by in situ electrochemical/contact angle measurements. A small droplet of the electrolyte solution, pH = 7.0, was placed on the monolayer-modified electrode used as a working electrode, and two thin wires (Pt and Ag) were introduced into

(44) (a) Bokris, J. O'M.; Reddy, A. K. N.; Gamboa-Aldeco, M. *Modern Electrochemistry*, 2nd ed., v.2A; Kluwer Academic: New York, 2000. (b) Delahay, P. *Double Layer and Electrode Kinetics*; Wiley-Interscience: New York, 1965.

(45) (a) Lahann, J.; Mitragotri, S.; Tran, T.-N.; Kaido, H.; Sundaram, J.; Choi, I. S.; Hoffer, S.; Somorjai, G. A.; Langer, R. *Science* **2003**, *299*, 371−374. (b) Wang, X.; Kharitonov, A. B.; Katz, E.; Willner, I. *Chem. Commun.* **2003**, 1542−1543.

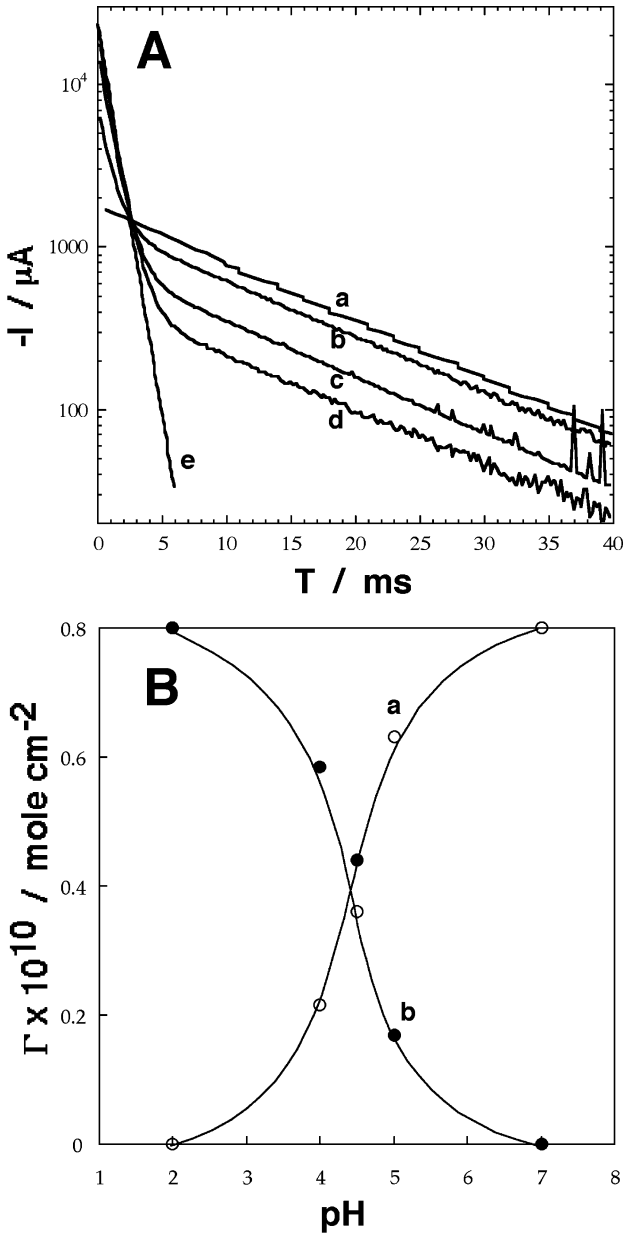

Figure 9. (A) Cathodic current transients observed upon application of a potential step from −0.33 to −0.53 V on the rotaxane-functionalized Au electrode that was prebiased at −0.33 V for 10 s at various pH values: (a) pH = 7.0; (b) pH = 5.0; (c) pH = 4.5; (d) pH = 4.0; (e) pH = 2.0. All data were recorded in 0.1 M Britton−Robinson buffer at variable pH under Ar. (B) The surface coverage of the cyclophane (**2**) populations revealing the slow electron-transfer kinetics (a) and the fast electron-transfer kinetics (b) derived from the chronoamperometric measurements.

the droplet to operate as a counter electrode and a quasi-reference electrode, respectively. Contact angles were measured upon applying potentials corresponding to −0.33 and −0.53 V on the modified electrode, yielding the cyclophane (**2**) in its oxidized and reduced states, respectively. Figure 10A, pictures a and b, shows the images of the droplet upon applying potentials corresponding to −0.33 and −0.53 V on the electrode, respectively. The measured contact angle of the droplet changes reversibly from ca. 55° when the cyclophane is in its oxidized state to ca. 105° when it is reduced, Figure 10B. These results are consistent with the fact that the oxidized cyclophane yields a hydrophilic interface, whereas the reduced state of the cyclophane forms a hydrophobic interface. In a control experiment application of the potentials corresponding to −0.33 and −0.53 V on the electrode consisting of the molecular strings without threaded cyclophane (**2**) resulted in similar contact angles corresponding to 98° ± 2°. In a further control experiment we applied the two potentials (−0.33 and −0.53 V) on the electrode that includes an acidic aqueous droplet (pH = 2) on the rotaxane-modified electrode. We find that the contact angle is ca. 42° and is independent of the applied potential. In acidic solution the molecular strings are protonated and thus exhibit hydrophilic character. Under these conditions the cyclophane (**2**) is translocated toward the electrode surface and the electron-transfer resulting in the reduction of **2** and its oxidation occur near the electrode surface without altering its steric position. We thus conclude that the observed contact angle reflects mainly the hydrophilic properties of the protonated brush of the molecular strings exposed to the solution.

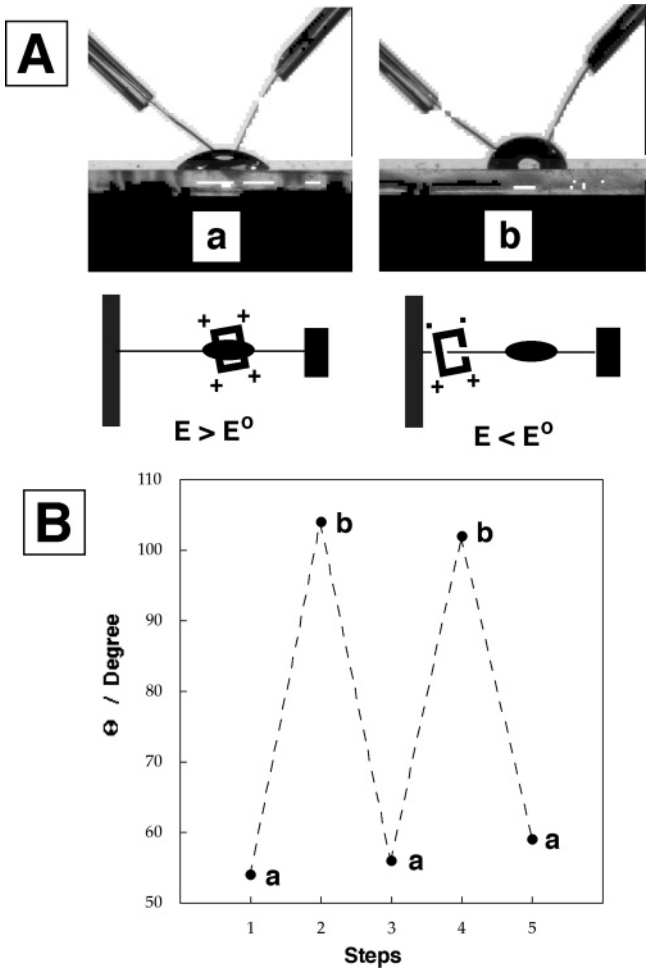

Figure 10. (A) In situ electrochemical/contact angle measurements performed on the rotaxane-functionalized Au electrode using a droplet of 0.1 M phosphate buffer, pH = 7.0, upon biasing the modified electrode at different potetials: (a) E_{bias} = −0.33 V; (b) E_{bias} = −0.53 V. (B) Electrochemically induced reversible changes of the contact angle values upon biasing the modified electrode at (a) E_{bias} = −0.33 V and (b) E_{bias} = −0.53 V. The data were recorded under Ar.

Conclusions

The present study has addressed the assembly of an electrochemically activated molecular shuttle on a "molecular string" in a rotaxane structure associated with an electrode surface. The study has demonstrated the use of chronoamperometry and

impedance spectroscopy to follow the position of the redox-active molecular shuttle on the "molecular string". The use of impedance spectroscopy to probe the dynamic structural changes of the molecular shuttle is particularly interesting since it provides information on the electromechanically driven capacitance changes of the monolayer. A further important aspect of the study includes direct determination of the rate constants corresponding to translocation of the molecular shuttle on the "molecular string". The translocation rate is found to be controlled by the direction of the movement, and the different rates are controlled by chemical and electrostatic interactions that prevail in the molecular structures. In general, the double-potential step chronoamperometric experiments provide a new and useful technique to follow and characterize electrochemically driven molecular mechanical translocations. We anticipate that this method could be applied to study molecular motions on "molecular strings" of higher complexity, e.g., strings that include several electrochemically active molecular shuttles or electrochemically activated π-donor binding sites.

Finally, demonstration that electrochemical shuttling of the redox-active cyclophane on the "molecular string" controls the hydrophobic/hydrophilic properties of the interface is of fundamental and, eventually, practical importance. The system adds a new structural element that controls the hydrophobicity/hydrophilicity of surfaces by means of electrically driven mechanical configurational/conformational changes of monolayer interfaces.[45a] Previous studies have demonstrated that electrochemical control of the interfacial properties of surfaces may be used to transport hydrophobic or hydrophilic liquids (e.g., in capillaries).[46] Thus, our study implies that directional molecular mechanical motion in supramolecular systems may be translated into controlled motion of bulk liquids in appropriate surface-modified containers.

Supporting Information Available: Nonsymmetrical shifts of the potentials corresponding to cathodic and anodic peak currents in the cyclic voltammograms of the rotaxane-functionalized electrode at different potential scan rates are discussed. The frequency changes measured by the quartz crystal microbalance technique upon stepwise modification of the electrode are presented. This material is available free of charge via the Internet at http://pubs.acs.org.

JA045465U

(46) Abbott, N. L.; Whitesides, G. M. *Langmuir* **1994**, *10*, 1493−1497.